BEAMFORMER ANALYSIS OF MEG DATA

Arjan Hillebrand and Gareth R. Barnes

The Wellcome Trust Laboratory for MEG Studies, Neurosciences Research Institute
Aston University, B4 7ET Birmingham, United Kingdom

In this chapter we provide a detailed description of a source reconstruction approach, beamforming, which was only recently introduced to electroencephalography (EEG) and magnetoencephalography (MEG) (Robinson and Vrba, 1999; van Veen *et al.*, 1997). As with any other source reconstruction method, a set of *a priori* assumptions are made so that a solution to the inverse problem can be obtained (e.g., Baillet *et al.*, 2001). The main assumption behind the beamformer approach is that no two distant cortical areas generate coherent local field potentials over long time scales; it has been shown empirically (Hillebrand *et al.*, 2005; Singh *et al.*, 2002) that this is a reasonable assumption set. We argue on the basis of anatomical and electrophysiological data why the beamformer assumption set, although simplistic, may indeed be quite plausible. We also illustrate when the assumptions might fail and make suggestions for improvements in the beamformer implementations. We conclude that beamforming is an exciting new approach to MEG source reconstruction that could provide another stepping stone on the route towards an appropriate assumption set with which to non-invasively image the brain.

I. Introduction

Magnetoencephalography (MEG) measures the magnetic fields outside the head created by electrical neuronal activity. The aim of many studies is to

INTERNATIONAL REVIEW OF NEUROBIOLOGY, VOL. 68
DOI: 10.1016/S0074-7742(05)68006-3

0074-7742/05 $35.00

subsequently determine the spatiotemporal characteristics of these neuronal sources on the basis of the extracranial recordings, which means that an inverse problem needs to be solved. The MEG inverse problem is theoretically insoluble; just as inferring a three-dimensional scene from a two-dimensional image is insoluble. However, we are able to interpret cinematic images because we make certain assumptions about the world (the size of people, the way shadows fall) that allow us to achieve a percept. In MEG we are searching for a similar set of assumptions on which to base algorithms to interpret the MEG data. Recent work has shown that a class of algorithms used to solve the MEG inverse problem produce functionally plausible and verifiable results. These algorithms make the assumption that no two distinct cortical areas are perfectly linearly correlated in their activation time series and it has been shown empirically that this assumption is often justified. First, the spatial concurrence of beamformer images of induced neuronal activity and the BOLD (blood oxygenation level dependent) functional magnetic resonance imaging (fMRI) response was demonstrated in a biological motion and a letter fluency task (Singh *et al.,* 2002) and more recently in a working memory task (Coppola *et al.,* 2004). Second, beamformer analysis has been applied successfully in various experimental paradigms, ranging from experiments involving primary visual, auditory, and somatosensory cortices as well as the use of more cognitively demanding paradigms (e.g., Fawcett *et al.,* 2004; Furlong *et al.,* 2004; Gaetz and Cheyne, 2003; Hashimoto *et al.,* 2001; Herdman *et al.,* 2003; Hobson *et al.,* 2005; Kamada *et al.,* 1998; Ploner *et al.,* 2002; Taniguchi *et al.,* 2000; Ukai *et al.,* 2002; also see Hillebrand *et al.,* 2005, for review).

One of the main advantages of beamformer analysis is that induced changes in cortical oscillatory power that do not result in a strong average-evoked response can be identified and localized. In particular, by using an active and control state, stimulus induced increases and decreases in cortical rhythms, known as event-related synchronization (ERS) and event-related desynchronization (ERD), respectively (Pfurtscheller and Lopes da Silva, 1999), can be quantified. Such changes in ongoing activity have been shown to play an important role in cognitive function (Arieli *et al.,* 1996; Basar *et al.,* 2001; Karakas *et al.,* 2000; Kenet *et al.,* 2003; Makeig *et al.,* 2002; Ringach, 2003), and consequently form the basis of many theories of consciousness (Engel *et al.,* 2001; Freeman, 2000; Llinás *et al.,* 1998; Singer, 1998; Tononi and Edelman, 1998).

Another advantage of beamformer analysis is that there is relatively little user interaction. The only parameters that a user needs to select are the size of the reconstruction grid, the time-frequency window over which to run the analysis, and optionally the amount of noise regularization. Importantly, there is no need to define the number of active sources *a priori*, since the beamformer output is computed for each voxel in the source-space independently and sequentially. The user friendliness of the technique makes it suitable for use in a clinical setting.

This chapter is divided in two main sections. In the first section we describe the basic algorithmic steps that compose the beamformer and the characteristics of the reconstructed image of neuronal activity. We restrict almost all of our discussion to the measurement of induced and not evoked electrical activity. The beamformer approach has been used successfully in many experimental settings, hinting at the validity of the assumptions behind the technique. In the second section of this chapter we develop a case for why the beamformer assumption set, although simplistic, may indeed be quite plausible.

II. Beamformer Basics

Beamforming techniques were developed for radar applications (van Veen and Buckley, 1988) to modify the sensitivity profile of fixed array radars, such that signals coming from a location of interest were received while signals coming from other locations were attenuated. This focusing is achieved by selectively weighting the contribution that each sensor makes to the overall beamformer output. Increasing the sensitivity to signals coming from a location of interest can obviously be exploited for the reconstruction of the neuronal sources generating EEG and MEG data (Fig. 1). The main assumption behind beamformer analysis is that no two macroscopic (extent of the order of mm^2) sources of neuronal activity are correlated (e.g., Robinson and Vrba, 1999; van Veen and Buckley, 1988). When sources are perfectly linearly correlated, the beamformer will recover very little or no power.

The recorded MEG signal at any time instant, $\mathbf{B}$, is related to the neuronal activity by the following equation (e.g., Hämäläinen and Ilmoniemi, 1984; Hämäläinen *et al.*, 1993; Singh *et al.*, 1984):

$$\mathbf{B} = \mathbf{LQ} \tag{1}$$

where the $N \times 1$ matrix $\mathbf{Q}$ is the strength of the neuronal activity, $\mathbf{L}$ is the so-called lead field matrix ($M \times N$), M is the number of sensors, and N is the number of elements in the pre-defined source-space.

The lead field is defined as the MEG signal that is produced by a source of unitary strength, and is completely determined by the sensor configuration, volume conductor model, and the source model. For simplicity, we will use a single sphere as a volume conductor model and an equivalent current dipole as a source model (see the following text for a discussion of the use of different source and head models), so that the lead field is only determined by the source and sensor locations/orientations and the sphere origin (Sarvas, 1987). Furthermore, we will assume for now that the orientation of the source is known.

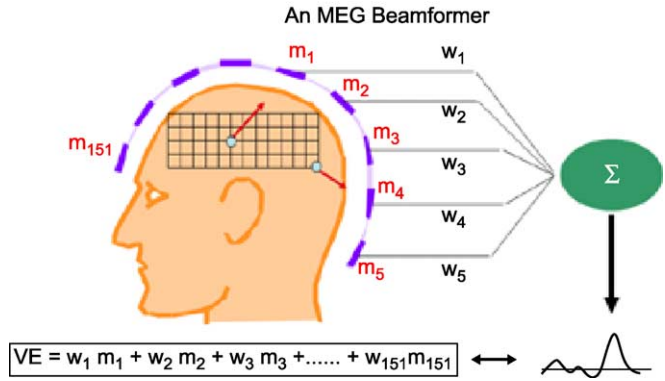

FIG. 1. Illustration of the main idea behind beamforming. The neuronal signal at a location of interest is constructed as the weighted sum of the MEG channels ($m_1 \ldots m_{151}$), forming a so-called virtual electrode (VE). The weights ($w_1 \ldots w_{151}$) are chosen so that only the signal from the location of interest contributes to the beamformer output, whereas the signal from noise sources is suppressed. A different set of weights is computed sequentially for each location in the brain, Figure courtesy of Dr. D. Cheyne, University of Toronto (modified).

Based on the measurements over time, $\mathbf{B}(t)$, one would like to determine the locations and strength of the neuronal activity. It can be shown that in its most general form (the generalized linear inverse) the neuronal activity at any latency can be expressed as (Mosher *et al.*, 2003):

$$\mathbf{Q} = \mathbf{C}_j \, \mathbf{L}^T \mathbf{C}_b^{-1} \mathbf{B} \tag{2}$$

with $\mathbf{C}_j$ as the source current covariance matrix and $\mathbf{C}_b$ as the data covariance matrix.

Differences between various source reconstruction algorithms arise from the different assumptions that are made about the source current covariance matrix (see Hillebrand *et al.*, 2005; Mosher *et al.*, 2003). In the case of the beamforming approach, it is assumed that all sources are uncorrelated, i.e., $\mathbf{C}_j$ is a diagonal matrix, and that each diagonal element in $\mathbf{C}_j$, corresponding to a location θ, can be related to the measured data as follows (Mosher *et al.*, 2003):

$$\sigma_\theta^2 = (\mathbf{L}_\theta^T \, \mathbf{C}_b^{-1} \, \mathbf{L}_\theta)^{-1} \tag{3}$$

Combining the two equations above gives:

$$Q_\theta = (\mathbf{L}_\theta^T \, \mathbf{C}_b^{-1} \, \mathbf{L}_\theta)^{-1} \, \mathbf{L}_\theta^T \, \mathbf{C}_b^{-1} \, \mathbf{B} = \mathbf{W}_\theta^T \, \mathbf{B} \tag{4}$$

Equation 3 is the crux of the beamformer algorithm. It is here that the source covariance $\mathbf{C}_j$ is estimated based on the data, and it is at this stage where the importance of the underlying assumptions becomes clear. The value of the diagonal element of $\mathbf{C}_j$ (Equation 3) determines the eventual power of any source

at this location. If all data covariance were due to a single source at location θ then equation 3 would be at a maximum. When there is a source at location θ, but it shares variance with another source having a different lead field, the estimated power at θ will decline. Van Veen *et al.* (1997) showed that the effect of correlated activity depends on the distance between the correlated sources. For a high correlation, the beamformer erroneously reconstructed a single source in between the two correlated closely spaced sources, whereas well-separated sources were almost completely cancelled. Importantly, it was shown that the beamformer was robust to partial correlation between sources. Moreover, a recent simulation study (Hadjipapas *et al.*, 2005), where these effects were quantified in terms of highly correlated yet transient source interaction, showed that in these cases the interdependencies of periodic sources were preserved and that phase-synchronization of interacting non-linear sources was not perturbed by the beamformer analysis. It has recently been proposed that the use of a higher-order covariance matrix might enable the reconstruction of strongly correlated activity with beamformers (Huang *et al.*, 2004).

It has recently been shown (Huang *et al.*, 2004) that equation 4 forms the basis of the different beamformer formulations currently used in the neuroimaging community (Barnes and Hillebrand,2003; Gross *et al.*, 2001; Robinson and Vrba, 1999; Sekihara *et al.*, 2001; Sekihara *et al.*, 2002; van Veen *et al.*, 1997). The various beamformer implementations differ only in how a statistical parametric image (SPM) of neuronal activity is computed and in how the problem of an unknown source orientation is dealt with. Regarding the orientation of each target source, we have so far assumed that the source orientation is known. In practice, one can perform a search for the orientation that optimizes the beamformer output (Robinson and Vrba, 1999; Fig. 1 in Hillebrand and Barnes, 2003) or compute the beamformer output for the two tangential orientation components (or all three orthogonal components in the case of EEG) and obtain the vector sum (Sekihara *et al.*, 2001; van Veen *et al.*, 1997). In this chapter we will use the word beamformer to describe variants of the linear constrained minimum variance (LCMV) algorithm described by van Drongelen *et al.* (1996) and Van Veen *et al.* (1997).

The beamformer output can be computed sequentially for all voxels in a predefined source space, forming an SPM. These images exhibit a non-uniform projection of sensor noise (the weights increase with depth, but the sensor level noise remains constant) throughout the volume (see Robinson and Vrba, 1999). Normalizing the beamformer output can compensate for this inherent bias. We will describe the normalization used by Robinson and Vrba (1999), although slightly different normalization approaches are also in use by other beamformer implementations (see Huang *et al.*, 2004, for review). Assume that the sensor noise covariance matrix, $\mathbf{\Sigma}$, is known, then the normalized beamformer output can be computed as (Robinson and Vrba, 1999):

$$Z_\theta^2 = \frac{P_\theta}{N_\theta} = \frac{\mathbf{W}_\theta{}^T \mathbf{C}_b \mathbf{W}_\theta}{\mathbf{W}_\theta{}^T \boldsymbol{\Sigma} \mathbf{W}_\theta} \tag{5}$$

with N_θ the power of the projected sensor noise and Z_θ the pseudo-Z statistic for location θ.

SPMs of pseudo- scores typically show a peak centered on the electrical source location. Note that only the noise sensitivity is required for the normalization and that, therefore, one could replace (given uniform sensor noise) the sensor noise covariance matrix with the identity matrix in the denominator of equation 5. This will only change the scaling of the SPM, but not the spatial information that it contains. Importantly, once the location of the neuronal activity is determined from the peaks in the SPM, one can still create an estimate of the time course of the neuronal activation using equation 4. This will give an unbiased estimate of source amplitude, but will contain projected sensor white noise that is dependent on source depth.

The normalization becomes redundant when an experiment contains different contrast windows, say an active and control condition. In this case, an SPM can be constructed from the statistical comparison of the source power in the different contrast windows (Barnes and Hillebrand, 2003; Vrba and Robinson, 2001b). Although the non-uniform sensor noise will affect the active and passive estimates of source power, it will not affect the statistical difference between them. Hence, the student's T-statistic can be computed as (Vrba and Robinson, 2001b):

$$T_\theta = \frac{\overline{P_\theta{}^{active}} - \overline{P_\theta{}^{control}}}{\sqrt{\sigma^2 / n_w}}, \tag{6}$$

with n_w estimates of source power in the contrast windows, active and control, and σ the pooled estimate of the standard deviation across these estimates. denotes the average value.

This provides a true T-statistic and the statistical probability for each voxel, therefore, can be computed (uncorrected for multiple comparisons). Alternatively, Vrba and Robinson (2001b) present a computationally efficient (the weight calculation stage can be skipped) statistic called the pseudo-T:

$$\mathrm{T}_\theta = \frac{\overline{P_\theta{}^{active}} - \overline{P_\theta{}^{control}}}{\overline{N_\theta{}^{active}} + \overline{N_\theta{}^{control}}}, \tag{7}$$

where N_θ is a noise estimate based on the projected sensor noise (see Equation 5).

Similarly, more sophisticated statistical measures can be computed for more complex experimental designs (e.g. Brookes *et al.*, 2004; Sabbah *et al.*, 2002).

In order to reduce the amount of sensor noise that is projected in the source space one can regularize the beamformer. In this case, the data covariance matrix is replaced by $\mathbf{C}_b + \mu\boldsymbol{\Sigma}$, where μ is a regularization parameter that

adjusts the trade-off between spatial selectivity and sensitivity to uncorrelated sensor noise. The spatial resolution of the beamformer images is highest when no regularization is applied, but the reconstructed neuronal activity is relatively noisy. In contrast, when the beamformer is fully regularized, the spatial resolution is low, but the reconstructed neuronal activity is less contaminated by projected sensor noise. In fact, the beamformer weights for a fully regularized beamformer are simply a scaled version of the lead field for that target voxel (Hillebrand and Barnes, 2003). That is, the beamformer output is simply a projection of the measurement vector onto the lead field for the target voxel (Hillebrand and Barnes, 2003; Vrba, 2002), known as signal space projection (SSP) (Tesche *et al.*, 1995). Interestingly, the fully regularized beamformer image, in this case, is linearly related to the dipole fit error surface (Hillebrand and Barnes, 2003).

A. Properties of Beamformer Images

To put the following sections into context it is worth reiterating some of the points made in the previous text. First, beamformers produce volumetric images of changes in electrical activity. These images are appealing as they look like fMRI images for which we already have a comprehensive battery of analysis tools (e.g., SPM, AFNI) for assessing significance of activation, performing region of interest analysis, and so on. The main difference between BOLD fMRI images and beamformer power change images is the smoothness. fMRI images have intrinsic, and more or less homogeneous, smoothness due to homogeneous scanner resolution throughout the volume. That is, the (for example, 10^5) voxels in a volumetric image are related only locally and only by smoothness due to limited scanner resolution, or deliberate smoothing to improve sensitivity. If one bears in mind that volumetric beamformer images derive entirely from the linear superposition of (150 or so) measurements, and yet that very high (potentially infinite) spatial resolution is achievable (see Fig. 2), it becomes clear that beamformer images cannot be homogeneously smooth. Smoothness can be defined as the linear correlation between the activity at adjacent voxels. In fMRI, for example, it can be estimated from the correlation between the noise at adjacent voxels remaining when experimental effects have been modeled out (Kiebel *et al.*, 1999). In the case of the beamformer, however, the relationships between adjacent voxels are directly related to the weight vectors which project to them (Barnes and Hillebrand, 2003). If the weight vectors at two voxels are identical, so will the beamformer output at those voxels. Examining the smoothness across the volume shows that it is minimal around source locations (Barnes and Hillebrand, 2003; Barnes *et al.*, 2004; Gross *et al.*, 2001, 2003; Vrba and Robinson, 2001a; van Veen *et al.*, 1997) giving locally very high spatial resolution. This raises a number of problems. First, how does one choose an adequate level for spatial

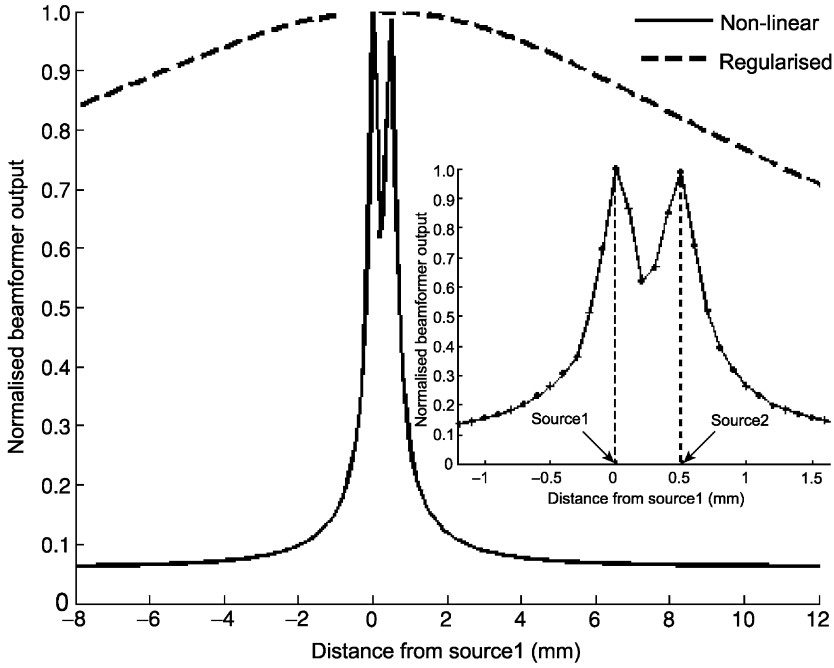

FIG. 2. Beamformer output for data from two sources separated by only 0.5 mm. The two original sources had a strength of 1,000 nAm, a tangential orientation, and were placed on a grid at the approximate location of the occipital lobe that extended in the other tangential direction. The temporal profile of the first source was a sinusoid at 20 Hz and was a cosine at the same frequency for the second source. The configuration of a 151-channel MEG system (CTF Systems Inc.; Vrba *et al.*, 1999) and a spherical head model was used for the computations of the lead fields. 100 epochs of MEG data were simulated with a per-channel white noise level of 90 fT rms (10 fT/$\sqrt{\text{Hz}}$, 81 Hz bandwidth) and 625 data samples were used for the source reconstruction (0.5 seconds). Note that the non-linear beamformer (Robinson and Vrba, 1999) can successfully separate the two sources, whereas the fully regularized beamformer (which corresponds to performing a dipole fit; Hillebrand and Barnes, 2003) reconstructs only a single source approximately halfway between the two original sources, demonstrating the high spatial resolution that is achievable with beamformers. In fact, this is the order of resolution required to resolve human ocular dominance columns (Horton *et al.*, 1990). Of course we realize that sources with such a high strength are unrealistic (by about two orders of magnitude), but with directed experimental designs and modest improvements in instrumentation such SNR is already available. For example, approximately two orders of magnitude in amplitude SNR could be gained with current technology by limiting the bandwidth to 1 Hz (factor of 9), using a recording system with SQUID white noise level of 5 fT/$\sqrt{\text{Hz}}$ (factor of 2), doubling the number of recording channels (factor of $\sqrt{2}$) and recording five times as many stimulus-related events (factor of $\sqrt{5}$).

sampling? Barnes *et al.* (2004) have addressed this empirically (Barnes *et al.*, 2004), while Gross *et al.* (2003) provide an analytical technique to estimate smoothness. In the limit, however, as SNR increases, the reconstructed source power will be largely reduced unless the true underlying sources fit the beamformer expectations

(the lead field is accurate) and lie precisely on the sampling grid. Second, for the same reason it is essential that in any region of interest analysis the target voxel is chosen at peaks in the beamformer image, as all those voxels around it (if it is a strong source) will be maximally different (Barnes and Hillebrand, 2003; Barnes *et al.*, 2004). It should also be noted that high spatial resolution does not imply accuracy and that sub-millimeter distinctions such as those demonstrated in Fig. 2 will only occur if the lead field profiles and, therefore, the source and head models are known exactly.

B. Voxel Level Statistics

Consider that a set of weights have been calculated that map the sensor channels to a particular source voxel (at particular orientation) and that this estimate of electrical activity is veridical. The null hypothesis is that on average, across epochs, there is no change in the electrical power at this location between active and passive intervals. In order to refute this hypothesis, we have tended to use bootstrapping or permutation tests (Durka *et al.*, 2004; Greenblatt and Pflieger, 2004; Graimann *et al.*, 2002). It is not yet clear whether these tests (which have large computing overheads) are strictly necessary but their advantage is that they do not rely on the assumption of normality (like the Student's T-test). So for the single voxel, a true probability of activation is straightforward to compute. If the experiment consists of an active and a control phase then the power changes in the active phase can be expressed as a percentage of the activity in the control phase (Fig. 3B). The main difference between bootstrapping and randomization approaches are that with bootstrapping the measured data is seen as a representative sample of the population from which the data came. It then endeavors to draw conclusions about this population, based on population parameters such as the mean and standard deviation. This is achieved by estimating the population parameters many times, each time based on a new representation that is constructed by re-sampling the original data, with replacement. In comparison, randomization approaches query whether measured differences between data distributions depend on the stimulus condition(s) or occurred by chance. This is tested by repeatedly re-assigning (i.e., sampling *without* replacement) the measured data to one of the stimulus categories and re-computing the differences between the data distributions for the different categories. The significance of measured differences is then assessed against the population of differences obtained from the randomized data. In the case of assessing the significance of an increase or decrease in power with respect to a baseline signal, bootstrapping (Fig. 3C) would estimate a confidence interval for the mean signal change, and based on this confidence interval one could then assess whether this change is significantly different from zero, at a certain confidence level (Graimann *et al.*,

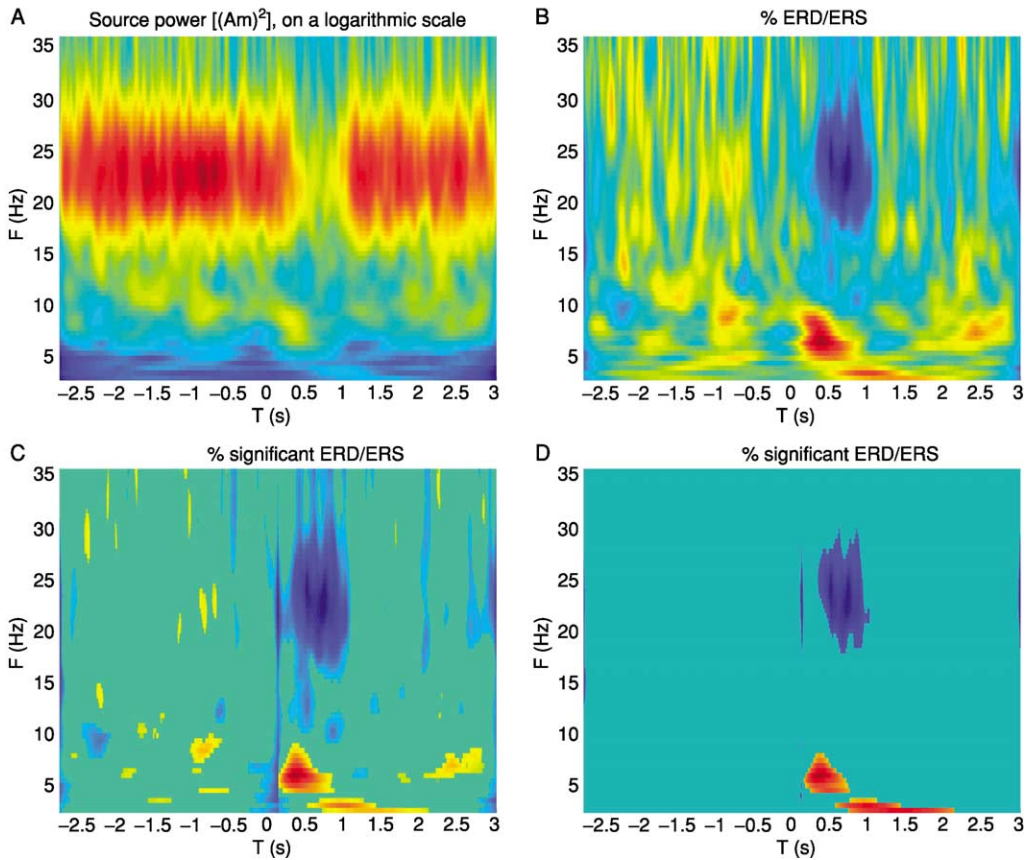
A
Source power [(Am)^2], on a logarithmic scale
B
% ERD/ERS
C
% significant ERD/ERS
D
% significant ERD/ERS
F (Hz)
T (s)
35
30
25
20
15
10
5
−2.5 −2 −1.5 −1 −0.5 0 0.5 1 1.5 2 2.5 3

2002). Randomization testing would estimate whether the amount of power change could have occurred by chance. The significance of the recorded power change is then obtained from the distribution of values for the re-shuffled data (Fig. 3D).

A typical time-frequency representation is based on the estimated signal energy at hundreds of different latencies and at many frequencies. Thousands of statistical tests, therefore, are performed in order to assess the significance of signal changes at each time-frequency point, resulting in a multiple comparisons problem. Conveniently, a correction for multiple comparisons can readily be performed when implementing randomization testing, as was described by Nichols and Holmes for fMRI analysis (2001). In the case of correcting for multiple comparisons in the time-frequency representation, one would estimate the largest change across the whole image for each permutation. Setting a certain significance level for the probability distribution for the maximum across the image then gives a threshold value for this maximum signal change. The measured maximum across the image, and consequently a*ny* measured change that is larger than this threshold value is significant, and corrected for multiple comparisons (Fig. 3D).

C. Subject Level Statistics

Currently we do not know of a satisfactory analytical solution to the problem of setting multiple comparison corrected levels of significance for beamformer images. Let us assume that the data covariance structure (and, hence, the beamformer smoothness) has been correctly estimated, in addition to which the source space has been adequately sampled. The problem with inhomogeneously smooth images is that the probability of, for example, 100 voxels in a smooth image section exceeding a threshold by chance may be the same as that of a

Fig. 3. (A) An example of wavelet analysis of the reconstructed neuronal activity in a region of interest in the somatosensory cortex. The passive phase was from −3 to 0 seconds and the active phase from 0 to 3 seconds (i.e., stimulus onset was at 0 seconds). Note the marked decrease in power in the 25 Hz band just after stimulus presentation (the figures are in arbitrary units; red corresponds to high values, blue to low values). The change in power with respect to the baseline (the passive phase) is often referred to as event-related desynchronization (ERD) when there is a decrease in power and as event-related synchronization (ERS) when there is an increase in power (Pfurtscheller and Lopes da Silva, 1999) (B). The significance of the ERD/ERS can be assessed with a bootstrap technique (C), showing only decreases/increases in power that were statistically significant, taking into account the variability of the power across all recorded epochs. The significance of the ERD/ERS can also be assessed using randomization testing (D). The advantage of randomization testing is that it is possible to correct for the multiple comparison problem.

single voxel being significant in an unsmooth region. Barnes and Hillebrand (2003) attempted to address this problem through Gaussian field-based methods developed for fMRI (Worsley *et al.*, 1999). The method is highly computationally intensive, as it requires smoothness calculation at potentially very high levels of sampling. It is possible, however, that this approach conflates two separate problems: the statistical correction and the accuracy of the image. Namely, the fact that large sections of beamformer images are smooth does not imply that the underlying electrical activity is smooth, but simply that it is of low power. Beamformer image smoothness, therefore, is for the most part artifactual and a consequence of having a limited number of channels that project to a large number of voxels.

A short-term solution might be to simply set the family wise error rate by adjusting for the maximal number of statistically independent voxels through a simple Bonferroni correction. The maximum number of independent voxels must be equal to the number of measurement channels. This is a conservative estimate, as the channels themselves are related through their overlapping sensitivity profiles, but may be a workable (and easily computable) solution until this problem is re-addressed.

Meanwhile, non-parametric methods, such as permutation testing have been successfully applied to provide true multiple comparison corrected p values for beamformer images (Cheyne *et al.*, 2003).

D. Group Level Statistics

For each time-frequency comparison and for each subject, beamformer analysis provides a volumetric image of neuronal activation or task-related changes in neuronal activation. These volumetric images are co-registered with each individual's MRI and, therefore, can be spatially normalized and averaged across a cohort of subjects (Park *et al.*, 2002; Singh *et al.*, 2002, 2003). This approach was first used in PET studies and subsequently applied to fMRI (see Friston, 2002, for review) in order to increase the signal-to-noise ratio (SNR). Statistical analysis on the group data highlights those responses that are consistent across subjects. Such an analysis can also be used to reveal statistically significant differences between different conditions or different cohorts of subjects, for example to compare a group of patients to a group of normal subjects.

MEG group analysis was first applied to beamformer data by Singh *et al.* (2002) using two different cognitive paradigms: a language task involving covert letter fluency and a biological motion direction discrimination task. Moreover, the exact same experimental designs were used for fMRI recordings, allowing for a direct comparison between the MEG and fMRI data. In both paradigms a close relationship between the location of the BOLD response and the location of

group-averaged ERD/ERS was revealed, suggesting that combining the results of fMRI and MEG beamformer analysis could reveal the relationship between the BOLD response and neuronal activity (see also Brookes *et al.,* 2005). However, these group-averaged beamformer images were simple averages without any attempt to form a statistical analysis of voxel and cluster significance. Such statistical methods are essential if meaningful comparisons are to be made between the group results for different cohorts of subject or modalities. Therefore, it was demonstrated in a follow-up paper (Singh *et al.,* 2003) how non-parametric methods can be applied to the SPMs to make robust statistical inferences about the group results. A conventional parametric approach and a non-parametric approach (see Nichols and Holmes, 2001, for a detailed description of non-parametric tests) were used to re-analyze the MEG data in the biological motion experiment referenced in the previous text. It was shown that non-parametric methods based on permutation testing out-perform conventional parametric tests using the classical T-statistic (for which no statistically significant clusters were found) and either Gaussian field theory (Worsley *et al.,* 1996) or Bonferroni correction for multiple comparisons.

III. Exploration of the Beamformer Assumptions

The beamformer could be thought of as a class of algorithm best suited to measuring a complex system in which, locally, processes are integrated (long-term coherent) but globally, they are segregated (long-term incoherent). In the following sections we will develop the argument that the brain is such a complex system. The first part of the argument (that of local integration) is not difficult to develop. Without such processes we would have no measurable aggregate local field potential (LFP) which to measure with MEG or EEG, and if adjacent neurons did not perform similar tasks a net change in oxygenation (and, hence, BOLD fMRI signal) would also fail to materialize. Indeed, a great deal of anatomical and functional information points towards high local connectivity. The more difficult argument to prove is that long-range integration is the exception rather than the rule. As a definition of terms, a local means a few millimeters, a global means a few centimeters; by short-term we mean milliseconds and long-term we mean hundreds of milliseconds.

Our argument in summary is this. Given that there is no pacemaker system in the brain, all neurons contribute equally to the development of LFPs. No two cortical columns have identical input connections and, therefore, cannot develop morphologically identical LFPs. Adjacent cortical columns are similarly connected and the LFPs generated will certainly be correlated to some degree. This similarity of connections, however, falls off with distance.

A. Anatomical Arguments

Cortical neurons are locally strongly grouped into mini-columns. These units are approximately 60 μm in diameter and contain approximately 100 pyramidal neurons which are bundled together (Mountcastle, 1997). These mini-columns, bound together by short-range horizontal connections, in turn form cortical columns or modules (sometimes called macro-columns) (Mountcastle, 1997). These columns are approximately 0.3 to 1.0 mm in diameter (Mountcastle, 1997; Peters and Yilmaz, 1993) and can be identified through the clusters of terminating thalamo- and cortico-cortical afferents (Mountcastle, 1997).

Local modules or columns are formed by virtue of their intrinsic lateral connectivity and clustered afferents from thalamo- and cortico-cortical mylenated fibers. The lateral connectivity of the cortex is clearly local (the probability that two cells are connected at a distance declines exponentially [Holmgren *et al.*, 2003]); is it possible that the mylenated fibers serve to provide constant long-range connectivity? Passingham *et al.* 2002 studied the correlation of connectivity patterns between cortical areas in the monkey. They found that the correlation between connectivity patterns between cortical areas declined with distance: neighboring areas had more similar connections but no two areas had the same connectivity, concluding that each area had a unique 'connectional fingerprint'. Similarly, Sporns *et al.* (2000a,b) examined the extrinsic connectivity between cortical areas in the cat and macaque. They found that connectivity patterns were similar to those of idealized complex systems, or small world networks, in which the majority of connections are local and global connections are sparse. Similar approaches have been used to show that the wiring length for existing cortical networks in the cat and macaque is close to minimal (Cherniak *et al.*, 2004).

Cortical areas seem to be uniquely interconnected, but is it possible that the thalamus adds a hierarchical layer of connectivity to the system? Evidence suggest that cortico-thalamic loops that could join disparate cortical areas actually only join areas that already have direct cortico-cortical projections (with limited exceptions; see Scannell, 1997). That is, thalamic nuclei, bearing in mind that there are no direct connections between them (Scannell *et al.*, 1999), do not appear to add to the connectivity that is not already present at a cortical level.

In summary, the case for local connectivity is strong: lateral connections between axonal and dendritic arbors are prevalent, which is coupled with the predominantly local profile of cortico-cortical mylenated projections (Cherniak *et al.*, 2004; Passingham *et al.*, 2002; Sporns *et al.*, 2000a). It should be noted that all of the arguments presented in the previous text are based on a mesoscopic description and we suggest that long-term, long-range linear and zero-lag interactions are rare. We do not imply that there are no long-range networks of individual neurons that are directly coupled, but for LFPs to look similar would require that thousands of their neighbors have identical inputs.

B. Electrical Arguments

Intra-cranial measurements seem to be conclusive in their findings that cortical rhythms have limited domains (Bullock *et al.*, 1995a; Shen *et al.*, 1999). Bullock *et al.* (1995b) describe 'local patterned mosaics of fluctuating coherence'; they (1995a) also describe estimated average local coherence between Electrocorticography (ECoG) electrodes at around 0.4 at 10-mm separation, dropping to <0.1 at 30 mm. Shen *et al.* 1999 report very similar ECoG data based on coherence of 10-minute segments of delta band activity[1]. There may also be a tendency for the size of the domain to be inversely proportional to the temporal frequency (Bullock *et al.*, 1995a; Nunez *et al.*, 2001). Such invasive data complements data from other species (Bullock and Mcclune, 1989; Freeman and Skarda, 1985; Leopold and Logothetis, 2003) and observations from some of the earliest intra-cranial recordings by Walter and colleagues (see Basar *et al.*, 1997). Hence, based on the intracranial EEG literature alone, the case for short-range coherence is compelling. It should be noted, however, that such data are normally collected over a densely sampled but confined cortical area (approximately 4 by 4 cm) and if there are long-range linear cortico-cortical interactions it may be that they extend beyond the size of these grids. Scalp EEG measures span the whole brain volume, but suffer from volume conduction and spatial low-pass filtering effects (Nunez *et al.*, 2001). That is, without unequivocal and precise source modeling, it is difficult, for example, to distinguish between the long-range zero-lag coherence of two sources and the single volume conduction effects of a single source. In addition, the spatially low-pass nature of the EEG means that what one sees on the scalp is a coarse spatial average of a number of underlying components (Cooper *et al.*, 1965; Nunez *et al.*, 2001).

Even when accounting for these factors through the use of conservative Laplacian estimates, some of the scalp EEG literature (Nunez, 1995; Nunez and Silberstein, 2000; Srinivasan, 1999) is still at odds with the intra-cranial data, especially in the alpha frequency band where relatively high coherence estimates (0.4 to 0.5) have been shown at distances of 15 to 20 cm. Robinson (2003) presents a theoretical model which resolves the apparent disparity between the scalp EEG and intra-cranial data, predicting a function of coherence fall off with distance which has resonance peaks at alpha and beta frequencies. Similarly, Nunez *et al.* (2001) makes a compelling philosophical case for the existence of both short- and long-range coherence in the EEG. In contrast, other scalp EEG studies have shown that neither the sensory motor beta (Andrew and Pfurtscheller, 1999) nor μ-rhythms (van Leeuwen *et al.*, 1978) are coherent across hemispheres.

[1] Shen *et al.* (1999), however, did observe occasional (approximately 1 pair in every 20), but repeatable, coherence levels of 0.3 to 0.4 for certain electrode pairings between 3 and 5 cm apart.

Besides the indirect beamformer evidence for predominantly local coherence (Hillebrand *et al.*, 2005), there are other MEG studies using non-beamformer methods that concur. Kilner *et al.* (2003) investigated the modulation in 15 to 30 Hz coherence between EMG and left and right sensory-motor cortices during a grip task. Although there was significant coherence between EMG and the contra-lateral sensory-motor cortex they concluded that there were independent oscillators in the two hemispheres. In an attempt to find inter-hemispheric coherence in the beta band, Nikouline *et al.* (2001) used a measure of phase synchrony (varying between 0 and 1) and found this to be on average low (0.1) and transiently high (0.3). Maybe such studies provide a clue to the disparity in the literature: perhaps if long-range mesoscopic coherence is a real cortical phenomenon, then it is also transient.

C. When Beamformer Analysis Fails

To date, we have found the main challenge to the beamformer assumption is in short latency evoked response studies where the sensory afferent volley to a number of disparate cortical areas (such as bilateral auditory cortices) is tightly time-locked to the onset of an external stimulus (leading to highly correlated distant sources). One approach to circumvent the problem with correlated sources is to select only those sensors that contain the signal from one of the sources. By using the sensors above each hemisphere separately, Herdman *et al.* (2003), for example, were able to successfully reconstruct bilateral sources underlying transient and steady-state auditory evoked responses, despite the similarity of their time courses of activation. As previously described, the beamformer passes only that part of the recorded signal that corresponds to the forward solution for a source at a target location. Selecting only a sub-set of sensors, therefore, will affect the signal-to-noise ratio of the reconstructed time courses, but does not introduce systematic errors in the reconstruction of the source locations. It is rare, however, for lead fields from related cortical areas to be as conveniently separable as those relating to auditory cortex.

Beamformer implementations generally use an equivalent current dipole at each target location as the source model for the computation of the lead fields. If this dipole model is inappropriate, say for an extended region of activity, and the true lead field deviates from that of a dipole, then the activity from the extended source will be suppressed by the beamformer (Vrba, 2002). It should be noted that the effect of inaccurate modeling is worse for data with high SNR and with more sensors, when the resolution of the beamformer is high enough to discriminate between the actual and modeled lead fields (Hillebrand and Barnes, 2003; Vrba, 2002). In such cases, more sophisticated source models (e.g., Jerbi *et al.*, 2002) could be used for the computation of the lead fields. For this same reason, it is important

to use an accurate head model for the computation of the lead fields. It has been shown for MEG that the accuracy obtained with a multisphere model is similar to that obtained with more computationally intensive head modeling using the boundary element method (Huang *et al.*, 1999). The effects of volume conduction on the EEG signal are more complicated and more realistic head models, therefore, are required for an accurate estimation of the lead fields. Although the ease of construction and computational efficiency of boundary and finite element models has improved over the last few years (e.g., Yvert *et al.*, 2001; Ermer *et al.*, 2001; Adde *et al.*, 2003; Tissari and Rahola, 2003; Zhang *et al.*, 2004), they are still not used routinely. This might explain the lack of beamformer usage in the EEG literature, despite the fact that beamformer analysis was first proposed for EEG data (van Drongelen *et al.*, 1996; van Veen *et al.*, 1997; Ward *et al.*, 1999).

Beamformers focus on regions of high source power and the resulting statistical images normally highlight changes in source power due to stimulus condition. That is, the current methods rely on congruence between the regions of largest power and those that are changing with the stimulus. If the sources that have largest power are those that change then the covariance calculation will be suboptimal (as the data has not remained stationary). On the other hand, if the regions that have largest power show no power modulation, beamformer weights will be focused on this region, displacing sensitivity from other brain regions with lower levels of activation but that do modulate with the stimulus condition. An interesting modification might be a beamformer that does not focus on (i.e., places nulls at) such constant power peaks.

In certain states of anesthesia, coma, and epilepsy, high coherence has been observed. For example, in epilepsy, it is not a healthy non-linear interaction that causes the electrical current in the cortex but an out of control cycling of the cells' control mechanisms. Bullock *et al.* (1995a) observed large increases in inter-electrode coherence during seizure, specifically at higher frequencies over longer electrode separations. Similarly, the "normal electrographic distinction" between cortical areas is eliminated in anesthesia (Jasper and Penfield, 1949). It is under these conditions that the assumptions underlying the beamformer formulation may prove to be in conflict with the actual state of the brain.

IV. Final Remarks

In this chapter we have attempted to provide an overview of a rapidly expanding set of algorithms for brain imaging. These algorithms make use of a previously unexplored and exciting assumption that no two distant cortical areas generate coherent LFPs over long time scales. There are bound to be cases (and diseases) in which this assumption fails and it is not the case that beamformers

provide us with a magic way to image the brain. However, the methods do bring to light a simple and surprisingly successful assumption set from which to build. Just as the equally simplistic assumptions behind dipolar models have proved their utility, and eventual limitations, the success of beamformer assumptions may not tell us exactly how the brain works, but it does provide us with new insights. We believe that beamformers provide another stepping stone on the route towards an appropriate assumption set with which to non-invasively image the brain.

References

Adde, G., Clerc, M., Faugeras, O., Keriven, R., Kybic, J., and Papadopoulo, T. (2003). Symmetric BEM formulation for the M/EEG forward problem. *Inf. Process Med. Imaging* **18,** 524–535.

Andrew, C., and Pfurtscheller, G. (1999). Lack of bilateral coherence of post-movement central beta oscillations in the human electroencephalogram. *Neurosci. Lett.* **273**(2), 89–92.

Arieli, A., Sterkin, A., Grinvald, A., and Aertsen, A.. (1996). Dynamics of ongoing activity: Explanation of the large variability in evoked responses. *Science* **273,** 1868–1871.

Baillet, S., Mosher, J. C., and Leahy, R. M. (2001). Electromagnetic brain mapping. *IEEE Signal Processing Magazine* **18**(6), 14–30.

Barnes, G. R., and Hillebrand, A. (2003). Statistical flattening of MEG beamformer images. *Hum. Brain Mapp.* **18**(1), 1–12.

Barnes, G. R., Hillebrand, A., Fawcett, I. P., and Singh, K. D. (2004). Realistic Spatial Sampling for MEG Beamformer Images. *Hum. Brain Mapp.* **23**(2), 120–127.

Basar, E., Schurmann, M., Basar-Eroglu, C., and Karakas, S. (1997). Alpha oscillations in brain functioning: An integrative theory. *Int. J. Psychophysiol.* **26**(1–3), 5–29.

Basar, E., Basar-Eroglu, C., Karakas, S., and Schürmann, M. (2001). Gamma, alpha, delta and theta oscillations govern cognitive processes. *Int. J. Psychophysiol.* **39,** 241–248.

Brookes, M. J., Gibson, A. M., Hall, S. D., Furlong, P. L., Barnes, G. R., Hillebrand, A., Singh, K. D., Holliday, I. E., Francis, S. T., and Morris, P. G. (2004). A general linear model for MEG beamformer imaging. *NeuroImage* **26**(1), 302–308.

Brookes, M. J., Gibson, A. M., Hall, S. D., Furlong, P. L., Barnes, G. R., Hillebrand, A., Singh, K. D., Holliday, I. E., Francis, S. T., and Morris, P. G. (2005). GLM-beamformer method demonstrates stationary field, alpha ERD and gamma ERS co-localisation with fMRI BOLD response in visual cortex. *NeuroImage* In Press.

Bullock, T. H., and Mcclune, M. C. (1989). Lateral coherence of the electrocorticogram: A new measure of brain synchrony. *Electroencephalogr. Clin. Neurophysiol.* **73**(6), 479–498.

Bullock, T. H., Mcclune, M. C., Achimowicz, J. Z., Iragui-Madoz, V. J., Duckrow, R. B., and Spencer, S. S. (1995a). EEG coherence has structure in the millimeter domain: Subdural and hippocampal recordings from epileptic patients. *Electroencephalogr. Clin. Neurophysiol.* **95**(3), 161–177.

Bullock, T. H., Mcclune, M. C., Achimowicz, J. Z., Iragui-Madoz, V. J., Duckrow, R. B., and Spencer, S. S. (1995b). Temporal fluctuations in coherence of brain waves. *Proc. Natl. Acad. Sci. USA* **92**(25), 11568–11572.

Cherniak, C., Mokhtarzada, Z., Rodriguez-Esteban, R., and Changizi, K. (2004). Global optimization of cerebral cortex layout. *Proc. Natl. Acad. Sci. USA* **101**(4), 1081–1086.

Cheyne, D., Gaetz, W., Garnero, L., Lachaux, J. P., Ducorps, A., Schwartz, D., and Varela, F. J. (2003). Neuromagnetic imaging of cortical oscillations accompanying tactile stimulation. *Brain Res. Cogn. Brain Res.* **17**(3), 599–611.

Cooper, R., Winter, A. L., Crow, H. J., and Walter, W. G. (1965). Comparison of subcortical, cortical and scalp activity using chronically indwelling electrodes in man. *Electroencephalogr. Clin. Neurophysiol.* **18,** 217–228.

Coppola, R., Calicotte, J. H., Holroyd, T., Verchinski, B. A., Sust, S., and Weinberger, W. J. (2004). MEG activation comparison to fMRI BOLD for a working memory task. Proceedings Biomag 2004, Boston (Abstr.).

Durka, P. J., Zygierewicz, J., Klekowicz, H., Ginter, J., and Blinowska, K. J. (2004). On the statistical significance of event-related EEG desynchronization and synchronization in the time-frequency plane. *IEEE Trans. Biomed. Eng.* **51**(7), 1167–1175.

Ermer, J. J., Mosher, J. C., Baillet, S., and Leahy, R. M. (2001). Rapidly recomputable EEG forward models for realistic head shapes. *Phys. Med. Biol.* **46,** 1265–1281.

Fawcett, I. P., Barnes, G. R., Hillebrand, A., and Singh, K. D. (2004). The temporal frequency tuning of human visual cortex investigated using synthetic aperture magnetometry. *NeuroImage* **21**(4), 1542–1553.

Freeman, W. J. (2000). Mesoscopic neurodynamics: From neuron to brain. *J. Physiol. Paris.* **94**(5–6), 303–322.

Freeman, W. J., and Skarda, C. A. (1985). Spatial EEG patterns, non-linear dynamics and perception: The neo-Sherringtonian view. *Brain Res.* **357**(3), 147–175.

Friston, K. J. (2002). *A short history of statistical parametric mapping in functional neuroimaging.* Technical report, Wellcome Department of Imaging Neuroscience, ION, UCL.

Furlong, P. L., Hobson, A. R., Aziz, Q., Barnes, G. R., Singh, K. D., Hillebrand, A., Thompson, D. G., and Hamdy, S. (2004). Dissociating the spatio-temporal characteristics of cortical neuronal activity associated with human volitional swallowing in the healthy adult brain. *NeuroImage* **22**(4), 1447–1455.

Gaetz, W. C., and Cheyne, D. O. (2003). Localization of human somatosensory cortex using spatially filtered magnetoencephalography. *Neurosc. Lett.* **340,** 161–164.

Graimann, B., Huggins, J. E., Levine, S. P., and Pfurtscheller, G. (2002). Visualization of significant ERD/ERS patterns in multichannel EEG and ECoG data. *Clin. Neurophysiol.* **113,** 43–47.

Greenblatt, R. E., and Pflieger, M. E. (2004). Randomization-based hypothesis testing from event-related data. *Brain Topogr.* **16**(4), 225–232.

Gross, J., Kujala, J., Hämäläinen, M., Timmermann, L., Schnitzler, A., and Salmelin, R. (2001). Dynamic imaging of coherent sources: Studying neural interactions in the human brain. *PNAS* **98**(2), 694–699.

Gross, J., Timmermann, L., Kujala, J., Salmelin, R., and Schnitzler, A. (2003). Properties of MEG tomographic maps obtained with spatial filtering. *NeuroImage* **19**(4), 1329–1336.

Hadjipapas, A., Hillebrand, A., Holliday, I. E., Singh, K. D., and Barnes, G. R. (2005). Assessing interactions of linear and nonlinear neuronal sources using MEG beamformers: A Proof of Concept. *Clin. Neurophysiol.* **116**(6), 1300–1313.

Hashimoto, I., Kimura, T., Iguchi, Y., Takino, R., and Sekihara, K. (2001). Dynamic activation of distinct cytoarchitectonic areas of the human SI cortex after median nerve stimulation. *NeuroReport* **12**(9), 1891–1897.

Hämäläinen, M., Hari, R., Ilmoniemi, R. J., Knuutila, J., and Lounasmaa, O. V. (1993). Magnetoencephalography—theory, instrumentation, and applications to noninvasive studies of the working human brain. *Rev. Mod. Phys.* **65**(2), 413–497.

Hämäläinen, M. S., and Ilmoniemi, R. J. (1984). "Interpreting measured magnetic fields of the brain: Estimates of current distributions. Rep. TKK-F-A559" Helsinki University of Technology, Helsinki.

Herdman, A. T., Wollbrink, A., Chau, W., Ishii, R., Ross, B., and Pantev, C. (2003). Determination of activation areas in the human auditory cortex by means of synthetic aperture magnetometry. *NeuroImage* **20,** 995–1005.

Hillebrand, A., and Barnes, G. R. (2003). The use of anatomical constraints with MEG beamformers. *NeuroImage* **20**(4), 2302–2313.

Hillebrand, A., Singh, K. D., Holliday, I. E., Furlong, P. L., and Barnes, G. R. (2005). A new approach to neuroimaging with magnetoencephalography. *Hum. Brain Mapp.* **25**(2), 199–211.

Hobson, A. R., Furlong, P. L., Worthen, S. F., Hillebrand, A., Barnes, G. R., Singh, K. D., and Aziz, Q. (2005). Real-time imaging of human cortical activity evoked by painful esophageal stimulation. *Gastroenterology* **128**(3), 610–619.

Holmgren, C., Harkany, T., Svennenfors, B., and Zilberter, Y. (2003). Pyramidal cell communication within local networks in layer 2/3 of rat neocortex. *J. Physiol.* **551**(Pt 1), 139–153.

Horton, J. C., Dagi, L. R., McCrane, E. P., and de Monasterio, F. M. (1990). Arrangement of ocular dominance columns in human visual cortex. *Arch. Ophthalmol.* **108**(7), 1025–1031.

Huang, M. X., Shih, J. J., Lee, R. R., Harrington, D. L., Thoma, R. J., Weisend, M. P., Hanlon, F., Paulson, K. M., Li, T., Martin, K., Miller, G. A., and Canive, J. M. (2004). Commonalities and differences among vectorized beamformers in electromagnetic source imaging. *Brain Topogr.* **16** (3), 139–158.

Huang, M. X., Mosher, J. C., and Leahy, R. M. (1999). A sensor-weighted overlapping-sphere head model and exhaustive head model comparison for MEG. *Phys. Med. Biol.* **44,** 423–440.

Jasper, H., and Penfield, W. (1949). Electrocorticograms in man: Effect of voluntary movement upon the electrical activity of the precentral gyrus. *Arch für Psychiatrie und Zeitschrift* **183,** 163–174.

Jerbi, K., Mosher, J. C., Baillet, S., and Leahy, R. M. (2002). On MEG forward modeling using multipolar expansions. *Phys. Med. Biol.* **47,** 523–555.

Kamada, K., Kober, H., Saguer, M., Möller, M., Kaltenhäuser, M., and Vieth, J. (1998). Responses to silent Kanji reading of the native Japanese and German in task subtraction magnetoencephalography. *Cog. Brain Res.* **7,** 89–98.

Karakas, S., Erzengin, Ö. U., and Basar, E. (2000). A new strategy involving multiple cognitive paradigms demonstrate that ERP components are determined by the superposition of oscillatory responses. *Clin. Neurophysiol.* **111,** 1719–1732.

Kenet, T., Bibitchkov, D., Tsodyks, M., Grinvald, A., and Arieli, A. (2003). Spontaneously emerging cortical representations of visual attributes. *Nature* **425,** 954–956.

Kiebel, S. J., Poline, J. B., Friston, K. J., Holmes, A. P., and Worsley, K. J. (1999). Robust smoothness estimation in statistical parametric maps using standardized residuals from the general linear model. *NeuroImage* **10**(6), 756–766.

Kilner, J..M, Salenius, S., Baker, S. N., Jackson, A., Hari, R., and Lemon, R. N. (2003). Task-dependent modulations of cortical oscillatory activity in human subjects during a bimanual precision grip task. *NeuroImage* **18**(1), 67–73.

Leopold, D. A., and Logothetis, N. K. (2003). Spatial patterns of spontaneous local field activity in the monkey visual cortex. *Rev. Neurosci.* **14**(1–2), 195–205.

Makeig, S., Westerfield, M., Jung, T-P., Enghoff, S., Townsend, J., Courchesne, E., and Sejnowski, T. J. (2002). Dynamic brain sources of visual evoked responses. *Science* **295,** 690–694.

Mosher, J. C., Baillet, S., and Leahy, R. M. (2003). Equivalence of linear approaches in bioelectromagnetic inverse solutions. *IEEE Workshop on Statistical Signal Processing*. Sep 28–Oct 1, 2003, St. Louis, Missouri (Abstr.).

Mountcastle, V. B. (1997). The columnar organization of the neocortex. *Brain* **120**(4), 701–722.

Nichols, T. E., and Holmes, A. P. (2001). Nonparametric permutation tests for functional neuroimaging: A primer with examples. *Hum. Brain Mapp.* **15,** 1–25.

Nikouline, V. V., Linkenkaer-Hansen, K., Huttunen, J., and Ilmoniemi, R. J. (2001). Interhemispheric phase synchrony and amplitude correlation of spontaneous beta oscillations in human subjects: A magnetoencephalographic study. *NeuroReport* **12**(11), 2487–2491.

Nunez, P. L. (1995). Neocortical dynamics and human EEG rhythms Oxford University Press, New York.

Nunez, P. L., and Silberstein, R. B. (2000). On the relationship of synaptic activity to macroscopic measurements: Does co-registration of EEG with fMRI make sense. *Brain Topogr.* **13**(2), 79–96.

Nunez, P. L., Wingeier, B. M., and Silberstein, R. B. (2001). Spatial-temporal structures of human alpha rhythms: Theory, microcurrent sources, multiscale measurements, and global binding of local networks. *Hum. Brain Mapp.* **13,** 125–164.

Park, H-J., Kwon, J. S., Youn, T., Pae, J. S., Kim, J-J., Kim, M-S., and Ha, K-S. (2002). Statistical parametric mapping of LORETA using high density EEG and individual MRI: Application to mismatch negativities in schizophrenia. *Hum. Brain Mapp.* **17,** 168–178.

Passingham, R. E., Stephan, K. E., and Kotter, R. (2002). The anatomical basis of functional localization in the cortex. *Nat. Rev. Neurosci.* **3**(8), 606–616.

Peters, A., and Yilmaz, E. (1993). Neuronal organization in area 17 of cat visual cortex. *Cereb. Cortex* **3** (1), 49–68.

Pfurtscheller, G., and Lopes da Silva, F. H. (1999). Event-related EEG/MEG synchronization and desynchronization: Basic principles. *Clin. Neurophysiol.* **110,** 1842–1857.

Ploner, M., Gross, J., Timmermann, L., and Schnitzler, A. (2002). Cortical representation of first and second pain sensation in humans. *PNAS* **99**(19), 12444–12448.

Ringach, D. L. (2003). States of mind. *Nature* **425,** 912–913.

Robinson, P. A. (2003). Neurophysical theory of coherence and correlations of electroencephalographic and electrocorticographic signals. *J. Theor. Biol.* **222**(2), 163–175.

Robinson, S. E., and Vrba, J. (1999). Functional neuroimaging by synthetic aperture magnetometry (SAM). *In* "Recent Advances in Biomagnetism" (Yoshimoto T., Kotani M., Kuriki S., Karibe H., and Nakasato N., Eds.), pp. 302–305. Tohoku Univ. Press, Sendai.

Sabbah, P., Zana, F., Nioche, C., and Cordoliani, Y. S. (2002). Using a bidimensional t test to compare simultaneous activations in functional brain MRI. *J. Clinl. Imag.* **26,** 77–80.

Sarvas, J. (1987). Basic mathematical and electromagnetic concepts of the biomagnetic inverse problem. *Phys. Med. Biol.* **32**(1), 11–22.

Scannell, J. W. (1997). Determining cortical landscapes. *Nature* **386**(6624), 452.

Scannell, J. W., Burns, G. A., Hilgetag, C. C., O' Neil, M. A., and Young, M. P. (1999). The connectional organization of the cortico-thalamic system of the cat. *Cereb. Cortex.* **9**(3), 277–299.

Sekihara, K., Nagarajan, S., Poeppel, D., Marantz, A., and Miyashita, Y. (2002). Application of an MEG eigenspace beamformer to reconstructing spatio-temporal activities of neural sources. *Hum. Brain Mapp.* **15,** 199–215.

Sekihara, K., Nagarajan, S. S., Poeppel, D., Marantz, A., and Miyashita, Y. (2001). Reconstructing spatio-temporal activities of neural sources using an MEG vector beamformer technique. *IEEE Trans. Biomed. Eng.* **48**(7), 760–771.

Shen, B., Nadkarni, M., and Zappulla, R. A. (1999). Spectral modulation of cortical connections measured by EEG coherence in humans. *Clin Neurophysiol.* **110**(1), 115–125.

Singh, K. D., Barnes, G. R., and Hillebrand, A. (2003). Group imaging of task-related changes in cortical synchronisation using non-parametric permutation testing. *NeuroImage* **19**(4), 1589–1601.

Singh, K. D., Barnes, G. R., Hillebrand, A., Forde, E. M. E., and Williams, A. L. (2002). Task-related changes in cortical synchronization are spatially coincident with the hemodynamic response. *NeuroImage* **16,** 103–114.

Singh, M., Doria, D., Henderson, V. W., Huth, G. C., and Beatty, J. (1984). Reconstruction of images from neuromagnetic fields. *IEEE Transac. Nuclear Sci.* **31**(1), 585–589.

Sporns, O., Tononi, G., and Edelman, G. M. (2000a). Connectivity and complexity: The relationship between neuroanatomy and brain dynamics. *Neural Netw.* **13,** 909–922.

Sporns, O., Tononi, G., and Edelman, G. M. (2000b). Theoretical neuroanatomy: Relating anatomical and functional connectivity in graphs and cortical connection matrices. *Cereb. Cortex.* **10**(2), 127–141.

Srinivasan, R. (1999). Spatial structure of the human alpha rhythm: Global correlation in adults and local correlation in children. *Clin. Neurophysiol.* **110**(8), 1351–1362.

Taniguchi, M., Kato, A., Fujita, N., Hirata, M., Tanaka, H., Kihara, T., Ninomiya, H., Hirabuki, N., Nakamura, H., Robinson, S. E., Cheyne, D., and Yoshimine, T. (2000). Movement-related desynchronization of the cerebral cortex studied with spatially filtered magnetoencephalography. *NeuroImage* **12,** 298–306.

Tesche, C. D., Uusitalo, M. A., Ilmoniemi, R. J., Huotilainen, M., Kajola, M., and Salonen, O. (1995). Signal-space projections of MEG data characterize both distributed and well-localized neuronal sources. *Electroencephalogr. Clin. Neurophysiol.* **95,** 189–200.

Tissari, S., and Rahola, J. (2003). A precorrected-FFT method to accelerate the solution of the forward problem in magnetoencephalography. *Phys. Med. Biol.* **48**(4), 523–541.

Ukai, S., Shinosaki, K., Ishii, R., Ogawa, A., Mizuno-Matsumoto, Y., Inouye, T., Hirabuki, N., Yoshimine, T., Robinson, S. E., and Takeda, M. (2002). Parallel distributed processing neuroimaging in the Stroop task using spatially filtered magnetoencephalography analysis. *Neurosci. Lett.* **334,** 9–12.

van Drongelen, W., Yuchtman, M., van Veen, B. D., and van Huffelen, A. C. (1996). A spatial filtering technique to detect and localize multiple sources in the brain. *Brain Topogr.* **9**(1), 39–49.

van Leeuwen, W. S., Wieneke, G., Spoelstra, P., and Versteeg, H. (1978). Lack of bilateral coherence of mu rhythm. *Electroencephalogr. Clin. Neurophysiol.* **44**(2), 140–146.

van Veen, B. D., and Buckley, K. M. (1988). Beamforming: A versatile approach to spatial filtering. *IEEE Acoustics, Speech, and Signal Processing Magazine* **5,** 4–24.

van Veen, B. D., van Drongelen, W., Yuchtman, M., and Suzuki, A. (1997). Localization of brain electrical activity via linearly constrained minimum variance spatial filtering. *IEEE Trans. Biomed. Eng.* **44**(9), 867–880.

Vrba, J. (2002). Magnetoencephalography: The art of finding a needle in a haystack. *Physica C* **368,** 1–9.

Vrba, J., Anderson, G., Betts, K., Burbank, M. B., Cheung, T., Cheyne, D., Fife, A. A., Govorkov, S., Habib, F., Haid, G., Haid, V., Hoang, T., Hunter, C., Kubik, P. R., Lee, S., McCubbin, J., McKay, J., McKenzie, D., Nonis, D., Paz, J., Reichl, E., Ressl, D., Robinson, S. E., Schroyen, C., Sekatchev, I., Spear, P., Taylor, B., Tillotson, M., and Sutherling, W. (1999). 151-channel whole-cortex MEG system for seated or supine positions. *In* "Recent Advances in Biomagnetism" (T. Yoshimoto, M. Kotani, S. Kuriki, H. Karibe, and N. Nakasato, Eds.), pp. 93–96. Tohoku Univ. Press, Sendai.

Vrba, J., and Robinson, S. E. (2001a). Differences between synthetic aperture magnetometry (SAM) and linear beamformers. *In* "12th International Conference on Biomagnetism" (J. Nenonen, R. J. Ilmoniemi, and T. Katila, Eds.), pp. 681–684. Helsinki Univ. of Technology, Espoo, Finland.

Vrba, J., and Robinson, S. E. (2001b). Signal processing in magnetoencephalography. *Methods* **25,** 249–271.

Ward, D-M., Jones, R. D., Bones, P. J., and Carroll, G. J. (1999). Enhancement of deep epileptiform activity in the EEG via 3-D adaptive spatial filtering. *IEEE Trans. Biomed. Eng.* **46**(6), 707–716.

Worsley, K. J., Andermann, M., Koulis, T., Mac Donald, D., and Evans, A. C. (1999). Detecting changes in nonisotropic images. *Hum. Brain Mapp.* **8**(2–3), 98–101.

Worsley, K. J., Marrett, S., Neelin, P., Vandal, A. C., Friston, K. J., and Evans, A. C. (1996). A unified statistical approach for determining significant signals in images of cerebral activation. *Hum. Brain Mapp.* **4,** 58–73.

Yvert, B., Crouzeix-Cheylus, A., and Pernier, J. (2001). Fast realistic modeling in bioelectromagnetism using lead-field interpolation. *Hum. Brain Mapp.* **14,** 48–63.

Zhang, Y. C., Zhu, S. A., and He, B. (2004). A second-order finite element algorithm for solving the three-dimensional EEG forward problem. *Phys. Med. Biol.* **49**(13), 2975–2987.